Journal of Magnetics 7(3), 115-125 (2002)

Thin Film Growth and Evaluation Method for Conventional Co-Cr Based Perpendicular Magnetic Recording Media: Problems and New Solutions

Shin Saito*, Fumikazu Hoshi, Daiji Hasegawa and Migaku Takahashi[1]

Department of Electronic Engineering, Graduate School of Engineering, Tohoku University, Aoba-yama 05, Aoba-ku, Sendai 980-8579 Japan

[1]New Industry Creation Hatchery Center, Tohoku University, Aoba-yama 04, Aoba-ku, Sendai 980-8579 Japan

(Received 9 September 2002)

We proposed a novel method to evaluate the magnetic properties of the initial layer and the columnar structure separately for CoCr-based perpendicular recording media. We show that the thickness of the initial layer and the intrinsic magnetocrystalline anisotropy of columnar structure can be quantitatively evaluated using the plotted product of perpendicular anisotropy to magnetic film thickness versus magnetic film thickness ($K_{u\perp}^{exp.} \times d_{mag.}$ vs. $d_{mag.}$ plot). Based on the analyses, it is found that: (1) compared with CoCrPtTa media, CoCrPtB media have relatively thin initial layer, and have fine grains with homogeneous columnar structure with *c*-plane crystallographic orientation; (2) CoCrPtB media can be grown epitaxially on Ru or CoCr/C intermediate layer, and as the result, the magnetic properties of the media within thin thickness region of $d_{mag.} \leq 20$ nm is significantly improved; (3) the key issue of material investigation for CoCr-based perpendicular recording media will be focused on how to fabricate *c*-plane-oriented columnar grains well isolated with nonmagnetic substance in epitaxial-growth media, while maintaining the thermal stability of the media.

Key words : CoCr-based perpendicular media, initial layer thickness, magnetocrystalline anisotropy, epitaxial growth

1. Introduction

Much attention has been paid for CoCr-based material to be used for perpendicular magnetic recording media, since it has a uniaxial magnetocrystalline anisotropy K_u^{grain} with condition of $K_u^{grain} > 2\pi M_s^2$ so that it has a potential to realize films with perpendicular magnetic anisotropy [1]. An ideal CoCr-based perpendicular magnetic recording media is considered to consist of assembly of single-domain magnetic grains with the *c*-axis parallel to the film normal direction. On the assumption that there exists magnetostatic coupling through demagnetizing field and no exchange coupling exists between magnetic grains in a medium, theoretically, the magnetic properties should take values such as $H_c/H_k = 1$, $S = M_r/M_s = 1$ and $\alpha = 1$ (Fig. 1). Here, H_c/H_k is coercivity normalized by magnetic anisotropy field, S is hysteresis loop squareness and α is gradient of hysteresis loop at coercivity, $4\pi(\Delta M/\Delta H)_{H=Hc}$. On the contrary, for experimentally fabricated media, the values of H_c/H_k and S are much smaller than 1 (e.g. Fig. 2). This phenomenon has been discussed for a long time, and is thought to be caused by intergranular exchange coupling [2, 3], magnetic reversal mode [4, 5], thermal agitation [6, 7] or initial layer [8, 9]. However, it is difficult to discuss the contribution of each factor separately. Prior to discussing this problem, we proceed to develop a way to realize a perpendicular media with perfectly eliminated initial layer. In this paper, we discuss an evaluation method to determine the magnetic properties for the initial layer and the *c*-plane-oriented columnar grains in a medium. Furthermore, we present a successful attempt of eliminating the initial layer of CoCr-based perpendicular media by epitaxially grown the media using $Co_{60}Cr_{40}$/C intermediate layer.

*Corresponding author: Tel: +81-22-217-7134, Fax: +81-22-263-9402, e-mail: ssaito@ecei.tohoku.ac.jp

2. Experimental Procedure and Analysis

CoNiCrTa, CoCrPtB and CoCrPtTa perpendicular thin film media were fabricated by dc magnetron sputtering method on 65-mm-diam glass substrates using the so-called ultra clean sputtering system [10]. The substrate was pre-heated by quartz lamp and the temperature was varied from R.T. to 300 °C. The sputtering was made

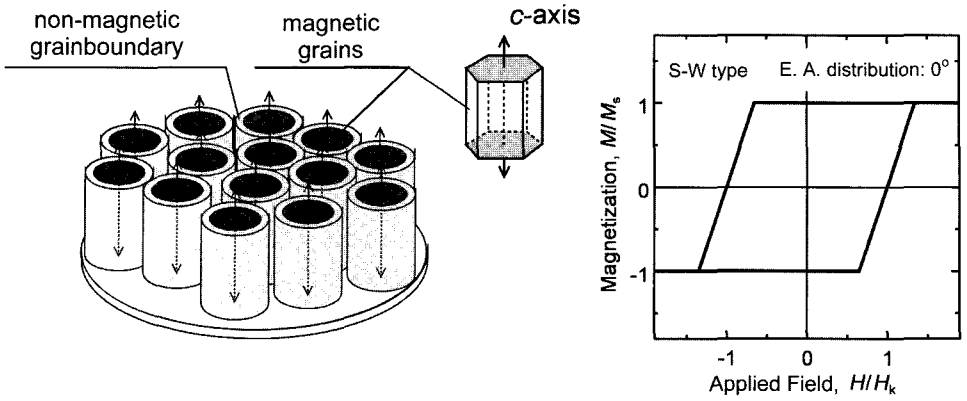

Fig. 1. Schematic view of an ideal CoCr-based perpendicular magnetic recording medium. The corresponding perpendicular magnetic hysteresis loop is also shown.

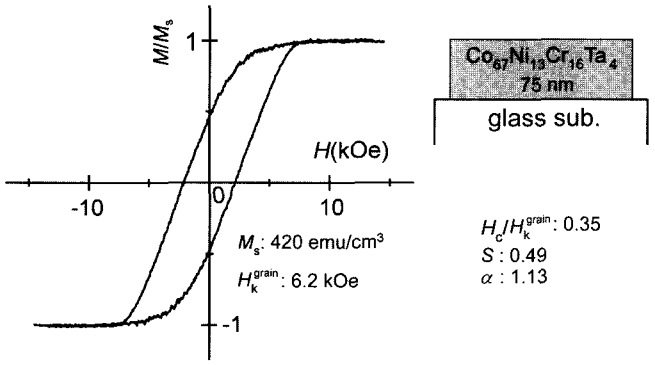

Fig. 2. Experimentally obtained perpendicular magnetic hysteresis loop for $Co_{67}Ni_{13}Cr_{16}Ta_4$ medium with thickness of 75 nm deposited on glass disk substrate. The magnetic properties for the media are shown in the figure.

under Ar pressure of 6.7×10^{-1} Pa. The film thickness of the magnetic layer was varied from 5 nm to 200 nm. The underlayer thickness was 7.5 nm for CoNiCrTa media or 25 nm for CoCrPtB and CoCrPtTa media, and the protective layer of carbon thickness was 7 nm, respectively. The film thickness was controlled by sputtering time.

The crystal structure of the media was examined by Grazing incident angle XRD method (in-plane XRD; $2\theta_\chi$ scan) [11] using Cu-Kα radiation. In the case of in-plane XRD, the incident angle was fixed at 0.4°, which corresponds to about 20 nm-thick penetration of X-ray from the incident surface. The microstructure was examined by transmission electron microscope (TEM) method.

The magnetic hysteresis loop was observed by VSM (swept field; 100 Oe/sec) and PKE (Polar Kerr Equipment, stepped field; 7 sec/each field). Polar Kerr hysteresis loop was examined from both the film surface side and the substrate side, with wavelength of 990 nm. To obtain a hysteresis loop measured from the substrate side, polar Kerr rotation was used, and the background Faraday rotation coming from the glass substrate was subtracted. Complex refractive index of the film, $n + i\kappa$, was evaluated by the rotating-analyzer ellipsometry. The difference between complex refractive index of right- and left-polarized light for the magnetic film, $\Delta n + i\Delta\kappa$, was consistently determined from n, κ, experimentally obtained saturation polar Kerr rotation and ellipticity, $\theta_K^{sat.}$ and $\eta_K^{sat.}$, by applying the matrix method [12].

The saturation magnetization and perpendicular magnetic anisotropy were evaluated by vibrating sample magnetometer (VSM) and high sensitive torque magnetometer, respectively. The torque curves were measured in various fields up to 20 kOe and were Fourier-analyzed to obtain the two-fold component which corresponds to the uniaxial anisotropy of the media. The saturated torque coefficient of the two-fold component, $L_{2\theta}^{sat.}$, was obtained by extrapolating the two-fold coefficient at each field vs. the inverse of magnetic field $1/H$ curve to $H \to \infty$. By taking account of the self-energy caused by demagnetizing field, the experimentally obtained total perpendicular magnetic anisotropy of the whole film, $K_{u\perp}^{exp.}$, can be expressed as

$$K_{u\perp}^{exp.} = L_{2\theta}^{sat.} + 2\pi M_s^2. \quad (1)$$

3. Results and Discussion

3.1. Microstructure along film thickness direction in CoCr-based perpendicular media

Figures 3 shows a bright-field image and electron diffraction patterns obtained by cross-sectional TEM for a $Co_{67}Ni_{13}Cr_{16}Ta_4$ medium with the thickness of 50 nm deposited on a glass substrate. In the bright field image, a layer structure with gray contrast can be clearly seen on the surface of the glass substrate and a columnar structure can be observed on top of the gray layer. According to the electron diffraction images, a ring pattern from the gray

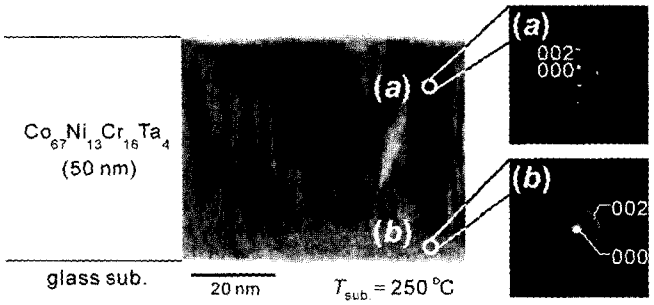

Fig. 3. Bright field image and electron diffraction patterns obtained by cross-sectional TEM analysis for $Co_{67}Ni_{13}Cr_{16}Ta_4$ medium with the thickness of 50 nm deposited directly on glass disk substrate. The diameter of electron probe is about 2 nm in selective area diffraction. Area (a) corresponds to the area from the columnar structure, and area (b) corresponds to the area from the initial layer.

zone (b) and a spot pattern from the columnar structure (a) were observed, respectively. These patterns correspond to the diffraction from the *c*-plane of the hcp structure. These facts indicate that the layer structure with the gray contrast consists of many nanocrystalline grains whose *c*-axes are three-dimensionally randomly oriented, and that the columnar structure consisted of hcp single grains with the *c*-plane parallel to the film plane. The same results were obtained for the medium with Ti underlayer. The gray zone is usually called the initial layer, and its nanocrystalline structure is very well known in perpendicular media studies [13]. Judging from the cross sectional TEM image, the average thickness of the initial layer, $d_{ini.}$ is about 10~15 nm for the media shown in Fig. 3.

3.2. Evaluation for separating the magnetic properties of columnar structure and initial layer

In following sections, we discuss about magnetic properties of media taking the existence of the columnar structure and the initial layer into account.

3.2.1. Magnetization curve

A "magnetization jump" is often observed in *M-H* loop of perpendicular media measured along the longitudinal direction [14]. This is because the easy axis of the columnar structure orients to the film normal direction, while the easy axis of the initial layer lies parallel to the film plane. In this way, although the perpendicular *M-H* loop looks to be homogeneous (e.g. see Fig. 2), local variation of magnetization process due to structural heterogeneity along film depth must exist. Therefore, we investigate the variation of perpendicular magnetization along the film thickness for perpendicular recording media using magneto-optical analysis [15, 16].

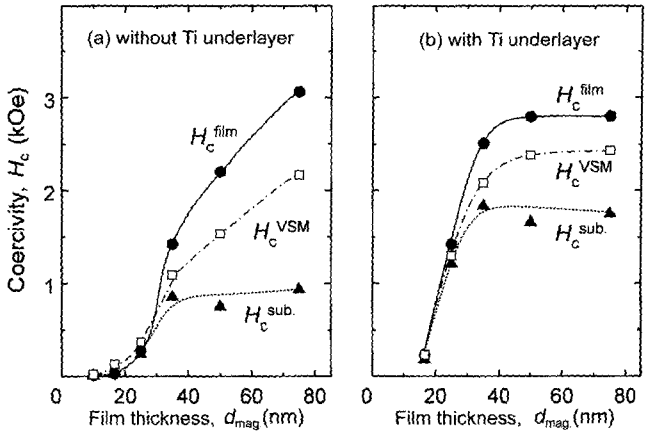

Fig. 4. Perpendicular coercivity, H_c, as a function of the magnetic film thickness, $d_{mag.}$ measured by PKE at 990 nm for $Co_{67}Ni_{13}Cr_{16}Ta_4$ media prepared (a) without and (b) with Ti underlayer, respectively. H_c^{film} corresponds to the H_c measured from the film surface side and $H_c^{sub.}$ corresponds to the H_c measured from the substrate side. H_c values measured by VSM (H_c^{VSM}) are also shown for comparison.

In Figs. 4, perpendicular coercivity, H_c, for $Co_{67}Ni_{13}Cr_{16}Ta_4$ media prepared (a) without and (b) with Ti underlayer is plotted against the magnetic film thickness, $d_{mag.}$ measured by PKE using a light with the wavelength of 990 nm. H_c^{film} corresponds to the H_c measured from the film surface side and $H_c^{sub.}$ corresponds to the H_c measured from the substrate side. H_c values measured by VSM (H_c^{VSM}) are also shown for comparison. For the films with $d_{mag.} \leq 25$ nm shown in Fig. 4(a), a slight difference in H_c between H_c^{film} and $H_c^{sub.}$ can be found. With increasing $d_{mag.}$ more than 25 nm, it is clearly seen that H_c^{film} is larger than $H_c^{sub.}$, and the difference between H_c^{film} and $H_c^{sub.}$ is 1.5 kOe at $d_{mag.} = 75$ nm. H_c^{VSM} shows a value between H_c^{film} and $H_c^{sub.}$. These facts mean that H_c of the initial layer is lower than that of the *c*-plane oriented columnar structure. The behavior of H_c against $d_{mag.}$ shows the same tendency for the films with Ti underlayer shown in Fig. 4(b). Note that the hysteresis loop measured from the substrate side does not exactly correspond to the hysteresis loop of the initial layer, since the penetration depth ($\lambda/2\pi\kappa \sim 28.7$ nm) of light with the wavelength of 990 nm is thicker than the thickness of the initial layer.

If the initial layer thickness can be determined by any other methods and assuming that the magnetization process of the columnar structure and the initial layer is homogenous and the interface between layers is flat, the hysteresis loop of the initial layer can be analytically derived by magneto-optical calculation. Here, as an example, we show the derivation of hysteresis loop for

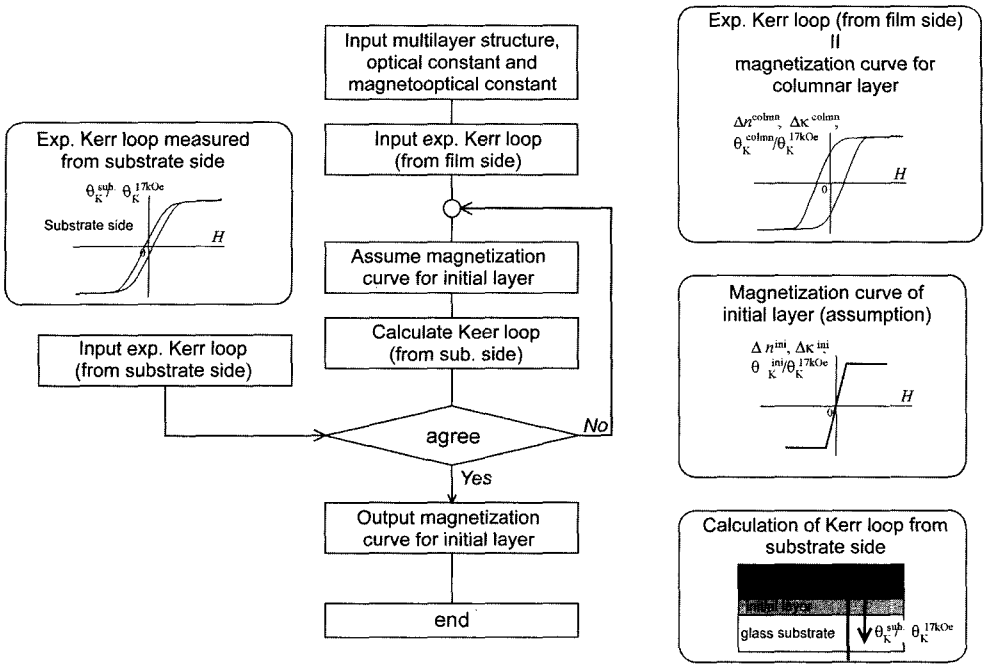

Fig. 5. A flowchart which shows the procedure to analytically derive the hysteresis loop of the initial layer.

$Co_{67}Ni_{13}Cr_{16}Ta_4$ medium with 50 nm-thickness shown in Fig. 3.

Figures 5 shows a flowchart for analytical derivation of magnetization curve for the initial layer. First, input the multilayer structure, the thickness, the optical and the magneto-optical constants for each layer. Then input experimental Kerr-loop data measured from the film side, which corresponds to the hysteresis loop of the columnar structure. Next, assume the hysteresis loop for the initial layer and carried out magneto-optical multi-layered calculation to derive a magnetic hysteresis loop observed from the substrate side. Then, input experimental Kerr-loop data measured from the substrate side and compare hysteresis loops from substrate side between calculated one and experimental one. If both hysteresis loops do not coincide, change the assumption of the hysteresis loop for the initial layer. Continue the calculation and the comparison until the calculated hysteresis loop agrees with the experimental one.

Figures 6(a) shows the calculated hysteresis loop of the initial layer broken line for $Co_{67}Ni_{13}Cr_{16}Ta_4$ medium (50 nm) fabricated directly on glass substrate. In the same figure, the experimentally obtained hysteresis loop of the columnar structure solid line is also shown for comparison. The media has an initial layer and a columnar structure with the thickness of 14.0 nm and 36.0 nm, respectively, determined by perpendicular magnetic anisotropy analysis. It is found that the initial layer shows no hysteresis in the loop, which indicates that the initial layer

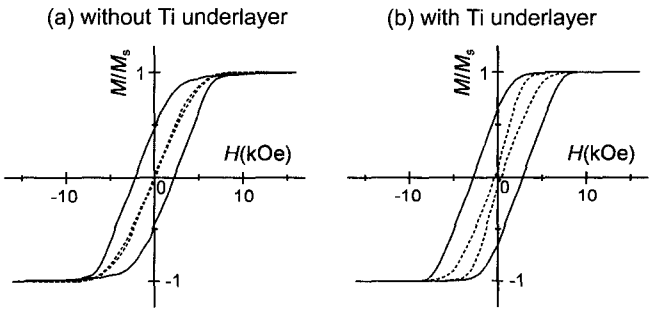

Fig. 6. Hysteresis loops of the initial layer broken line and the columnar structure solid line for $Co_{67}Ni_{13}Cr_{16}Ta_4$ medium with the thickness of 50 nm (a) without and (b) with Ti underlayer, respectively.

does not act as recording layer. Furthermore, since the initial layer is a continuous layer with strong exchange coupling, and the columnar structure is connected to the initial layer, the exchange coupling between grains in the columnar structure must arise, which must degrade the magnetic properties of the columnar structure. Fig. 6(b) shows hysteresis loops of the initial layer and the columnar structure for $Co_{67}Ni_{13}Cr_{16}Ta_4$ medium (50 nm) with Ti underlayer. It is found that the magnetic properties of the initial layer are still lower than that of the columnar structure.

3.2.2. Magnetic anisotropy field

For CoCr-based longitudinal recording media, it is

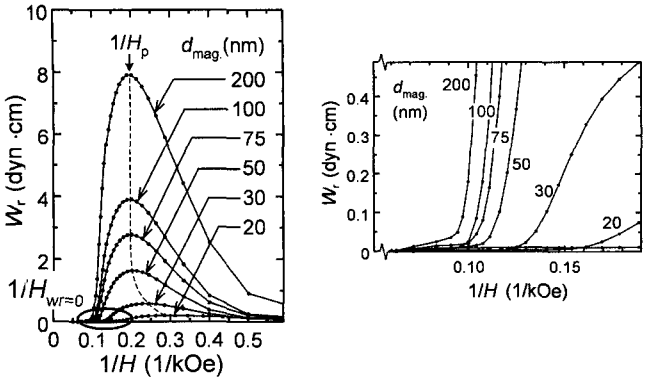

Fig. 7. Perpendicular rotational hysteresis loss, W_r, for $Co_{72}Cr_{16}Pt_8B_4$ media deposited on Ti underlayer with various magnetic film thicknesses, $d_{mag.}$, as a function of the inverse applied field, $1/H$.

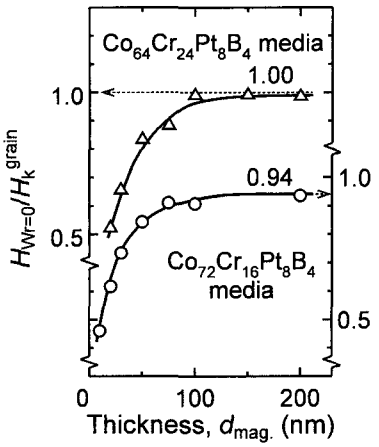

Fig. 8. Dependence of the magnetic field where rotational hysteresis loss vanishes, $H_{Wr=0}$, normalized by H_k^{grain}, $H_{Wr=0}/H_k^{grain}$, on magnetic film thickness, $d_{mag.}$, is shown for $Co_{72}Cr_{16}Pt_8B_4$ media (lower part) and $Co_{64}Cr_{24}Pt_8B_4$ media (upper part).

proposed that the magnetic field where rotational hysteresis loss (W_r) vanishes ($H_{Wr=0}$) corresponds to the magnetic anisotropy field (H_k) of magnetic grains [17, 18]. In the case of perpendicular recording media, if c-plane-oriented columnar grains consist of single domain particles with coherent rotation, $H_{Wr=0}$ should also correspond to H_k. In this section, the relationship between $H_{Wr=0}$ and H_k^{grain}, which was determined from $2K_u^{grain}/M_s$, is investigated by using CoCrPtB perpendicular media [19, 20]. Note that the magnitude of the magnetic anisotropy of the columnar structure is much larger compared with that of the initial layer. Therefore, it is safe to neglect the contribution from the initial layer effect in the range where rotational hysteresis loss of the columnar structure vanishes.

In Figs. 7, perpendicular rotational hysteresis loss, W_r, for $Co_{72}Cr_{16}Pt_8B_4$ media with various film thicknesses are shown as a function of the inverse applied field $1/H$. The measurement was started at large field (low $1/H$), and then the field was gradually decreased (increasing $1/H$). In all the media, W_r appears at low $1/H$, increases with increasing $1/H$, takes a maximum and then decreases. With increasing $d_{mag.}$, the maximum value of W_r increases, the inverse applied field, $1/H_p$, where W_r takes a maximum, and $1/H_{Wr=0}$ are shifted toward lower $1/H$ side. $H_{Wr=0}$ was determined by fitting W_r with a quadratic function in the range of $W_r^{max}/3$ to $W_r^{max}/20$.

In Fig. 8, the dependence of $H_{Wr=0}$ normalized by H_k^{grain}, $H_{Wr=0}/H_k^{grain}$, on magnetic film thickness, $d_{mag.}$ is shown for $Co_{72}Cr_{16}Pt_8B_4$ and $Co_{64}Cr_{24}Pt_8B_4$ media. For the $Co_{72}Cr_{16}Pt_8B_4$ media with $d_{mag.} = 10$ nm, $H_{Wr=0}/H_k^{grain}$ shows only a small value of 0.46. With increasing $d_{mag.}$, $H_{Wr=0}/H_k^{grain}$ gradually increases and saturates at the magnitude of 0.94 with $d_{mag.}$ over 100 nm. Almost the same tendency was observed in the $Co_{64}Cr_{24}Pt_8B_4$ media, in which $H_{Wr=0}/H_k^{grain}$ increases from a small value of 0.51 with $d_{mag.} = 20$ nm, and saturates at 1.00 with $d_{mag.}$ over 100 nm. Therefore, it was clarified that in thick $d_{mag.}$ region of $d_{mag.}$ over 100 nm, $H_{Wr=0}$ becomes close to about H_k^{grain} ($H_{Wr=0}/H_k^{grain} \approx 1$), and that in thin $d_{mag.}$ region of $d_{mag.}$ less than 100 nm, the thickness region of which is very important for application, $H_{Wr=0}$ is smaller than H_k^{grain}. From the result, we conclude that $2K_u^{grain}/M_s$ is the best method to evaluate magnetic anisotropy field of columnar structure in CoCr-based perpendicular media.

3.2.3. Magnetic anisotropy energy and thickness of initial layer

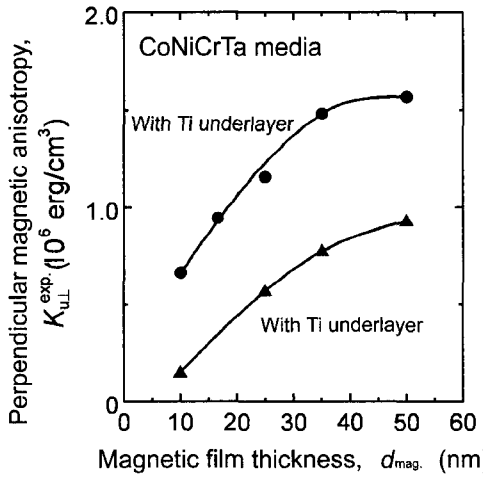

Fig. 9. Variation of the perpendicular magnetic anisotropy of the whole film, $K_{u\perp}^{exp.}$, as a function of magnetic film thickness, $d_{mag.}$, for $Co_{67}Ni_{13}Cr_{16}Ta_4$ media with and without Ti underlayer.

In this section, we will show that it is possible to quantitatively evaluate the intrinsic magnetocrystalline anisotropy of columnar structure, K_u^{grain}, and the thickness of the initial layer, $d_{ini.}$, using perpendicular torquemetry [21, 22].

Figure 9 shows the changes in the perpendicular magnetic anisotropy of the whole film, $K_{u\perp}^{exp.}$, as a function of magnetic film thickness, $d_{mag.}$ for $Co_{67}Ni_{13}Cr_{16}Ta_4$ media with and without Ti underlayer. In both media, for $d_{mag.}$ less than 35 nm, the $K_{u\perp}^{exp.}$ rapidly decreases with decreasing $d_{mag.}$. We emphasize that the result is not due to the variation of K_u^{grain} on $d_{mag.}$, but caused by the existence of the initial layer in the medium.

Concerning with the structural heterogeneity mentioned in Fig. 3, $K_{u\perp}^{exp.}$ can be considered as a summation of perpendicular magnetic anisotropy of both the columnar structure and the initial layer. In this case, the experimentally determined $K_{u\perp}^{exp.}$ can be expressed by the following equation:

$$K_{u\perp}^{exp.} = K_{u\perp}^{column} \times (V_{mag.}-V_{ini.})/V_{mag.}+K_{u\perp}^{ini.} \times V_{ini.}/V_{mag.}. \quad (2)$$

Where $K_{u\perp}^{column}$ and $K_{u\perp}^{ini.}$ are the average perpendicular magnetic anisotropy of the columnar structure and the initial layer, respectively, $V_{mag.}$ and $V_{ini.}$ are the volume of the whole magnetic film and the initial layer, respectively. By assuming that the interface between the initial layer and the columnar structure is flat, eq. (2) can be expressed as follows.

$$K_{u\perp}^{exp.} = K_{u\perp}^{column} \times (d_{mag.}-d_{ini.})/d_{mag.}+K_{u\perp}^{ini.} \times d_{ini.}/d_{mag.}. \quad (3)$$

As described in Fig. 3, since the initial layer consists of nanocrystalline grains whose c-axes are 3D randomly distributed, the whole ensemble of magnetocrystalline anisotropy of nanocrystalline grains, $K_{u\perp}^{ini.}$, is considered to be nearly zero.

$$K_{u\perp}^{ini.} = 0. \quad (4)$$

Furthermore, since the columnar structure consists of single crystal grains whose c-plane lies parallel to the film plane, the average perpendicular magnetic anisotropy of the whole columnar structures, $K_{u\perp}^{column}$, can be easily expected to be equal to the average magnetocrystalline anisotropy of each grains with uniaxial symmetry in the hexagonal structure, K_u^{grain}.

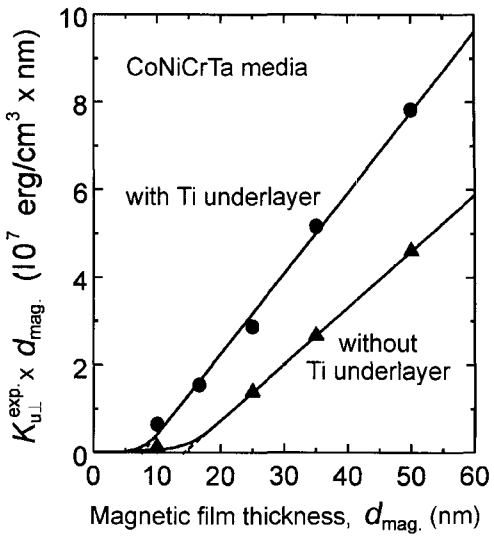

Fig. 10. $K_{u\perp}^{exp.} \times d_{mag.}$ vs. $d_{mag.}$ plot for $Co_{67}Ni_{13}Cr_{16}Ta_4$ media on glass substrate with and without Ti underlayer. Evaluated values of K_u^{grain} and $d_{ini.}$ for these media are summarized in Table 1.

$$K_{u\perp}^{column} = K_u^{grain}. \quad (5)$$

Therefore, eq. (3) can be rewritten into the following form:

$$K_{u\perp}^{exp.} \times d_{mag.} = K_u^{grain} \times (d_{mag.}-d_{ini.}). \quad (6)$$

Based on eq. (6), for perpendicular media composed of the initial layer and the columnar structure, we can simply derive K_u^{grain} and $d_{ini.}$ from $K_{u\perp}^{exp.} \times d_{mag.}$ vs. $d_{mag.}$ plot. By fitting the linear portion of $K_{u\perp}^{exp.} \times d_{mag.}$ vs. $d_{mag.}$ plot, K_u^{grain} can be uniquely determined from the gradient, and $d_{ini.}$ also can be determined from the intersection of the extended line of the with the $d_{mag.}$-axis.

In Fig. 10, $K_{u\perp}^{exp.} \times d_{mag.}$ is plotted as a function of $d_{mag.}$ for CoNiCrTa media on glass substrate with and without Ti underlayer. $K_{u\perp}^{exp.} \times d_{mag.}$ shows a linear correlation with $d_{mag.}$ in the range of $d_{mag.} > 25$ nm for the media without Ti underlayer and in the range of $d_{mag.} > 10$ nm for the media with Ti underlayer, respectively. Note that these experimental results correspond very well with the model expressed in eq. (6). The results shows that the initial layer is formed for both media, and that the intrinsic magnetocrystalline anisotropy of the columnar grains is constant independent of $d_{mag.}$. K_u^{grain} and $d_{ini.}$ determined from this method are 1.3×10^6 erg/cm^3 and 14.0 nm for

Table 1. K_u^{grain} and $d_{ini.}$ determined from $K_{u\perp}^{exp.} \times d_{mag.}$ vs. $d_{mag.}$ plot for $Co_{67}Ni_{13}Cr_{16}Ta_4$ media. The magnetic properties, M_s, H_c, S and a for the media are also summarized.

Media composition and layer structure	$d_{ini.}$ (nm)	K_u^{grain} (erg/cm^3)	M_s (emu/cm^3)	H_c (kOe) (50 nm)	S (50 nm)	α (50 nm)
$Co_{67}Ni_{13}Cr_{16}Ta_4$	14.0	1.29×10^6	420	1.5	0.58	1.19
$Co_{67}Ni_{13}Cr_{16}Ta_4$ / Ti (7.5 nm)	8.8	1.91×10^6	440	2.4	0.34	1.26

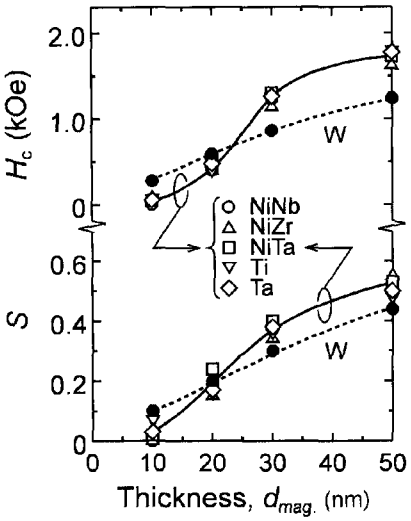

Fig. 11. Dependence of perpendicular magnetic properties H_c and S on magnetic film thickness, $d_{mag.}$, for $Co_{64}Cr_{24}Pt_8B_4$ media with amorphous underlayer, $Ni_{60}Nb_{40}$, $Ni_{60}Zr_{40}$, $Ni_{60}Ta_{40}$ and with high melting point underlayer Ta, W. Magnetic properties for the media with Ti underlayer are also shown.

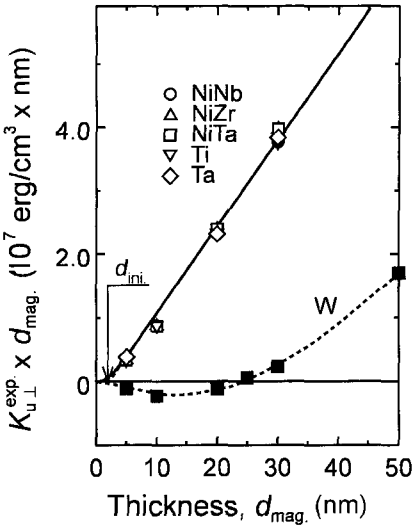

Fig. 12. $K_{u\perp}^{exp.} \times d_{mag.}$ vs. $d_{mag.}$ plot for $Co_{64}Cr_{24}Pt_8B_4$ media with amorphous underlayer, $Ni_{60}Nb_{40}$, $Ni_{60}Zr_{40}$, $Ni_{60}Ta_{40}$ and high melting point underlayer Ta, W. The $K_{u\perp}^{exp.} \times d_{mag.}$ for the media with Ti underlayer is also shown.

the media without underlayer, and 1.9×10^6 erg/cm^3 and 8.8 nm for the media with Ti underlayer, respectively. Results were summarized in Table 1.

3.3. Material investigation toward elimination of initial layer for CoCrPtM (M=B, Ta) media

In the following section, we discuss the effect of the magnetic layer and underlayer materials on the magnetic properties, the formation of the initial layer and the film microstructure in CoCrPt(B, Ta) perpendicular media by applying the evaluation method mentioned above.

3.3.1. Underlayer materials

For investigation of underlayer, materials with amorphous structure, $Ni_{60}Nb_{40}$, $Ni_{60}Ta_{40}$, $Ni_{60}Zr_{40}$ or materials with high melting point, Ta and W were chosen. For comparison, Ti underlayer was also investigated. Fig. 11 shows the thickness dependence of perpendicular magnetic properties H_c and S for $Co_{64}Cr_{24}Pt_8B_4$ media with various underlayer materials. Except for the media using W underlayer, all the media show similar magnetic properties dependence on $d_{mag.}$, independent of underlayer materials. On the other hand, in the case of the media using W underlayer, compared with the media using the other underlayer, H_c and S show relatively high values in the range 5 nm $\leq d_{mag.} \leq$ 20 nm, and show relatively low values in the range $d_{mag.} \geq$ 30 nm.

Figure 12 shows $K_{u\perp}^{exp.} \times d_{mag.}$ vs. $d_{mag.}$ plot for $Co_{64}Cr_{24}Pt_8B_4$ media with various underlayers. Except for the media using W underlayer, $K_{u\perp}^{exp.} \times d_{mag.}$ shows a linear correlation with $d_{mag.}$, and $d_{ini.}$ is evaluated as the value of 2.6 nm. On the other hand, in the case of the media using W underlayer, with increasing $d_{mag.}$, the sign of the value of $K_{u\perp}^{exp.} \times d_{mag.}$ changes from negative to positive and gradient of $K_{u\perp}^{exp.} \times d_{mag.}$ curve also changes. This is found to be brought by the variation of crystal texture of the columnar grains with $d_{mag.}$. According to in-plane XRD

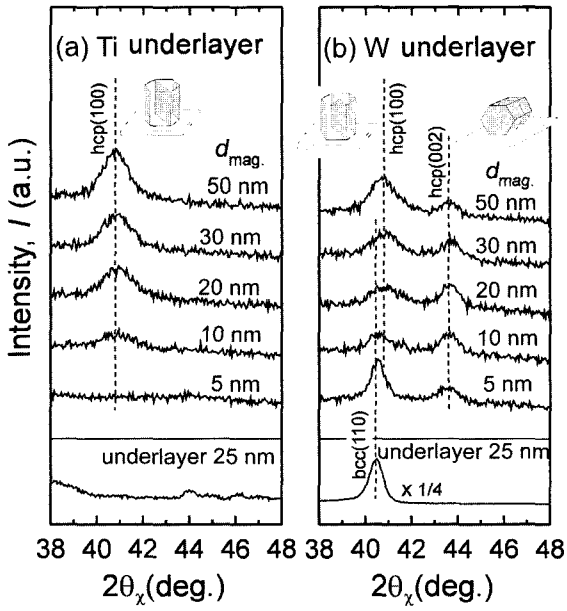

Fig. 13. In-plane XRD profiles for $Co_{64}Cr_{24}Pt_8B_4$ media with various magnetic film thickness, $d_{mag.}$, with (a) Ti underlayer and (b) W underlayer, respectively.

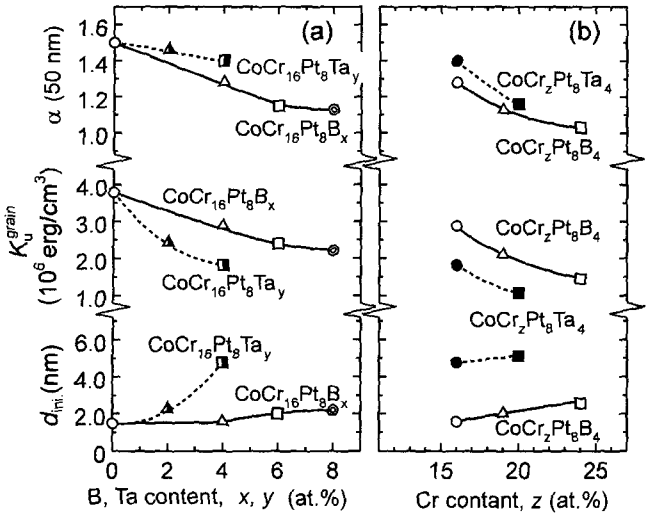

Fig. 14. Thickness of the initial layer, $d_{ini.}$, magnetocrystalline anisotropy, K_u^{grain}, and hysteresis loop gradient, α, plotted against the content of B, Ta or Cr for (a) $CoCr_{16}Pt_8B_x$, $CoCr_{16}Pt_8Ta_y$ and (b) $CoCr_zPt_8(B, Ta)_4$ media prepared on Ta underlayer, respectively. α was derived for the medium with the thickness of 50 nm.

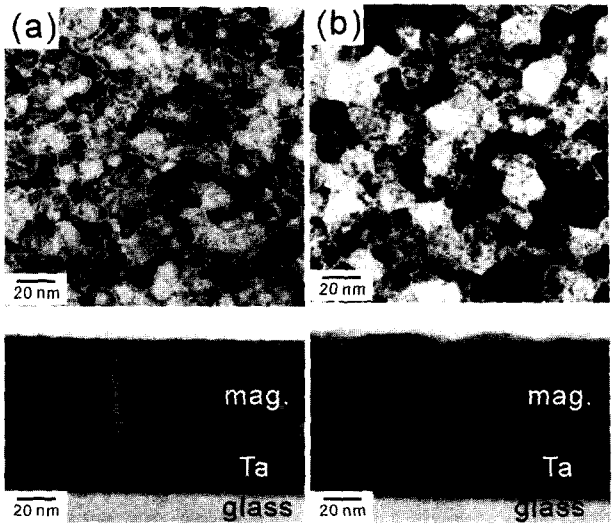

Fig. 15. Bright field images of plane view and cross-sectional view for the (a) $Co_{72}Cr_{16}Pt_8B_4$ medium and for the (b) $Co_{68}Cr_{20}Pt_8Ta_4$ medium with the thickness of 50 nm deposited on Ta underlayer.

analysis, for the media using W underlayer, with increasing $d_{mag.}$, the dominant orientation of columnar grains changes from the side-plane to c-plane of hexagonal structure (Fig. 13), whereas only *c*-plane-oriented grains are formed in the columnar structure for the other media.

3.3.2. Magnetic film composition

For investigation of magnetic film material, CoCrPtB and CoCrPtTa, which are popular magnetic materials used in longitudinal magnetic recording media for hard disk, were chosen [23].

Figures 14 (a) and (b) show $d_{ini.}$ plotted against the B, Ta or Cr content for $CoCr_{16}Pt_8B_x$, $CoCr_{16}Pt_8Ta_y$ and $CoCr_zPt_8$ (B, Ta)$_4$ media fabricated on Ta underlayer, respectively. In the case of the media with B addition (Fig. 14(a)), $d_{ini.}$ increases from 1.5 nm to 2.2 nm with increasing B from 0 at.% to 8 at.%. In the case of media with Ta addition (Fig. 14(a)), $d_{ini.}$ also increases from 1.5 nm to 4.8 nm with increasing Ta from 0 at.% to 4 at.%. It is well known that B or Ta addition is effective to realize magnetically isolated structure by segregation of Cr-rich phase in the grain boundary of magnetic layer in longitudinal media [24]. However, it was found out that these elements tend to enhance the formation of the initial layer in perpendicular media. Comparing CoCrPtB with CoCrPtTa media, with the same additional content of B or Ta, it was found that the CoCrPtB media has the thinner initial layer thickness. We also investigated $d_{ini.}$ for the $CoCr_zPt_8(B, Ta)_4$ media with various Cr content, z. As shown in Fig. 14(b), it was found that with increasing the Cr content z from 16 at.% to 24 at.% and from 16 at.% to 20 at.%, $d_{ini.}$ increased from 1.6 nm to 2.6 nm for B additional media and from 4.8 nm to 5.1 nm for Ta additional media, respectively.

To further investigate the initial growth structure dependence on the additional elements, microstructure observation by TEM method for the CoCrPtB and CoCrPtTa media were carried out. In Figs. 15(a) and (b), bright field images of plane view and cross-sectional view are shown for the media $Co_{72}Cr_{16}Pt_8B_4$ and $Co_{68}Cr_{20}Pt_8Ta_4$ with the $d_{mag.}$ of 50 nm, respectively. As seen in the plane view for the $Co_{72}Cr_{16}Pt_8B_4$ medium in Fig. 15(a), magnetic grains enclosed by the Cr-rich phase can be clearly observed. In the cross-sectional view, there exist an interface layer with light gray contrast between magnetic film and underlayer, and a columnar layer with stripe contrast just on the interface layer. The light gray contrast layer is considered to be the initial layer. On the other hand for the $Co_{68}Cr_{20}Pt_8Ta_4$ medium in Fig. 15(b), relatively larger grains are found in the plane view. From the cross-sectional view, it can be easily found that a relatively thick initial layer is formed. Furthermore, some grains grew with an inverted corn shape with increasing $d_{mag.}$, while the surrounding grains growth was suppressed. This fact is considered to be due to the different grain growth rate, originated from the disordered crystal orientation of initial grains. Comparing the surface roughness of the media, very smooth surface is realized for the $Co_{72}Cr_{16}$-

Pt_8B_4 medium, on the contrary for the $Co_{68}Cr_{20}Pt_8Ta_4$ medium, roughness with the period of the grain diameter, which is thought to be caused by the grain growth, is formed. Therefore, it was clarified that in the $Co_{72}Cr_{16}$-Pt_8B_4 medium, the initial growth region is relatively thin, and fine grains with homogeneous columnar structure with *c*-plane orientation are realized. On the other hand for the $Co_{68}Cr_{20}Pt_8Ta_4$ medium, the initial growth region is relatively thick, and the grain size distribution and surface roughness is large due to selective grain growth.

3.4. Perfect elimination of initial layer by epitaxial growth for CoCrPtB media

As we have discussed above, although $d_{ini.}$ could be reduced up to several nanometer thickness by using CoCrPtB material, the initial layer can not be completely eliminated. In this section, we introduce a successful attempt of perfect elimination of the initial layer by applying the epitaxial-growth technique using magnetic material with the composition of $Co_{67}Cr_{19}Pt_8B_4$. To realize the epitaxial growth of the magnetic layer, *c*-plane-oriented intermediate layer with hexagonal structure, Ru(3 nm) or $Co_{60}Cr_{40}$(20 nm)/C(1 nm), is deposited on Ti(25 nm) underlayer. Here, 1 nm of Carbon seedlayer underlying $Co_{60}Cr_{40}$(20 nm) intermediate layer plays a very important role to form Cr-deprived hcp grains with Cr segregation structure in $Co_{60}Cr_{40}$ layer without forming σ-phase grains [25, 26].

Figure 16 shows the dependence of perpendicular magnetic properties H_c and S on magnetic film thickness for $Co_{67}Cr_{19}Pt_8B_4$ media (*A*) without intermediate layer, (*B*) with Ru and (*C*) $Co_{60}Cr_{40}$/C intermediate layer, respectively. For the media *A*, in thin thickness region of $d_{mag.} \leq 10$ nm, H_c and S show low values of 0.1 kOe and 0.09, respectively. On the other hand, for the media *B* or *C*, H_c and S show relatively high values of about 1.4 kOe and 0.50, respectively, even when $d_{mag.} = 10$ nm. Especially for the media *C*, the maximum values of H_c and S are 3.5 kOe and 0.88 at $d_{mag.} = 30$ nm, higher than that of the media *B*.

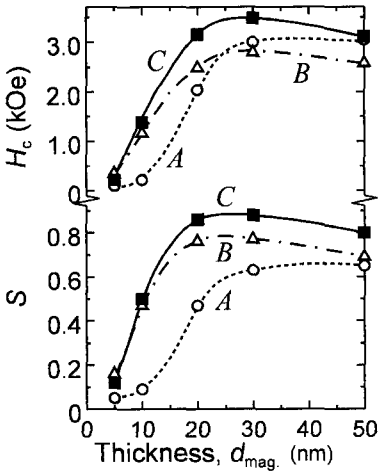

Fig. 16. Dependence of perpendicular magnetic properties H_c and S on magnetic film thickness, $d_{mag.}$, for $Co_{67}Cr_{19}Pt_8B_4$ media deposited on Ti underlayer (*A*) without, (*B*) with Ru(3 nm), and (*C*) $Co_{60}Cr_{40}$(20 nm)/C(1 nm) intermediate layer, respectively.

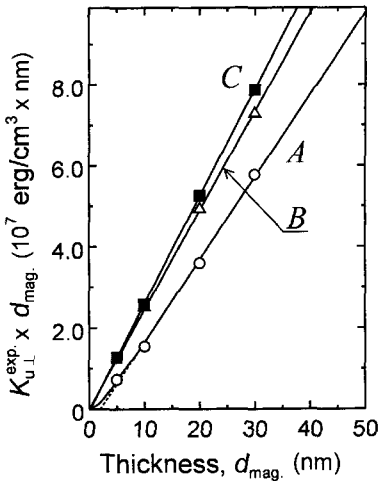

Fig. 17. $K_{u\perp}^{exp.} \times d_{mag.}$ vs. $d_{mag.}$ plot for $Co_{67}Cr_{19}Pt_8B_4$ media deposited on Ti underlayer (*A*) without, (*B*) with Ru(3 nm), and (*C*) $Co_{60}Cr_{40}$(20 nm)/C(1 nm) intermediate layer, respectively.

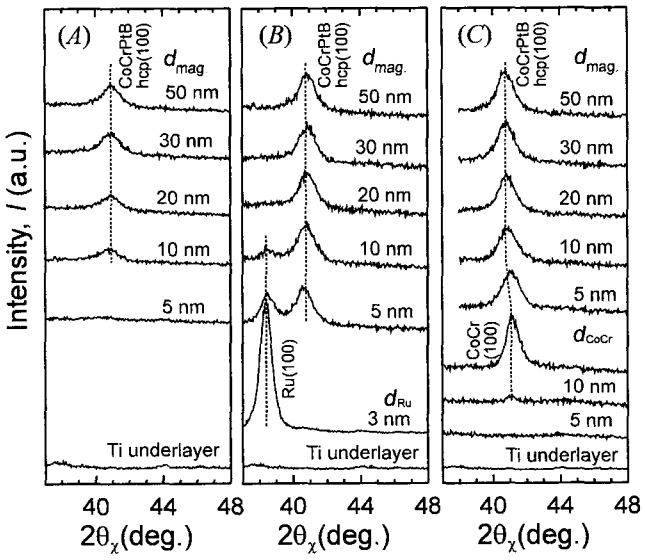

Fig. 18. In-plane XRD profiles for $Co_{67}Cr_{19}Pt_8B_4$ media deposited on Ti underlayer (*A*) without, (*B*) with Ru(3 nm), and (*C*) $Co_{60}Cr_{40}$(20 nm)/C(1 nm) intermediate layer, respectively. In-plane XRD profiles for Ti film, Ru film deposited on Ti underlayer, and $Co_{60}Cr_{40}$/C film deposited on Ti underlayer are also shown.

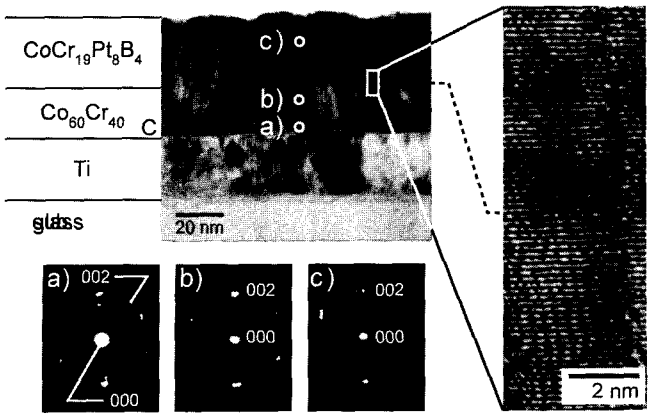

Fig. 19. A bright-field image and electron diffraction patterns obtained by cross-sectional TEM for (*C*) $Co_{67}Cr_{19}Pt_8B_4$ media with $Co_{60}Cr_{40}$/C intermediate layer. A high resolution image at the interface between $Co_{67}Cr_{19}Pt_8B_4$ magnetic layer and $Co_{60}Cr_{40}$ layer in this medium is also shown.

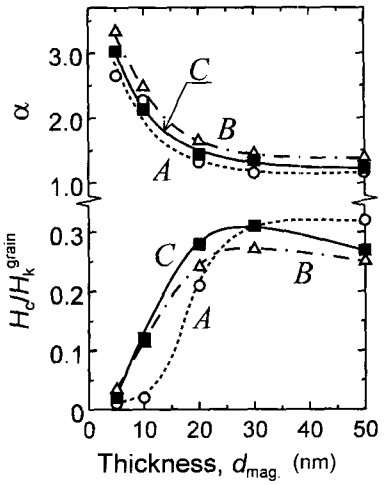

Fig. 20. Thickness dependence of (a) H_c/H_k^{grain} and (b) α for $Co_{67}Cr_{19}Pt_8B_4$ media (*A*) without intermediate layer, (*B*) with Ru and (*C*) $Co_{60}Cr_{40}$/C intermediate layer, respectively.

To verify the epitaxial growth, $K_{u\perp}^{exp.} \times d_{mag.}$ vs. $d_{mag.}$ plot, in-plane XRD analysis and TEM analysis were carried out.

Figure 17 shows $K_{u\perp}^{exp.} \times d_{mag.}$ vs. $d_{mag.}$ plot for $Co_{67}Cr_{19}$-Pt_8B_4 media (*A*) without intermediate layer, (*B*) with Ru and (*C*) $Co_{60}Cr_{40}$/C intermediate layer, respectively. The media *A* has the initial layer with the thickness of 2.0 nm. On the contrary, $K_{u\perp}^{exp.} \times d_{mag.}$ curves for the media *B* and *C* pass through the origin of the coordinate axes, which suggests the initial layer with low perpendicular magnetic anisotropy is completely eliminated.

Figures 18 show in-plane XRD profiles for $Co_{67}Cr_{19}$-Pt_8B_4 media (*A*) without intermediate layer, (*B*) with Ru and (*C*) $Co_{60}Cr_{40}$/C intermediate layer, respectively, with various film thickness. For the media *A* with $d_{mag.} = 5$ nm, a diffracted line can be hardly observed. However for the media *B* with Ru intermediate layer with $d_{mag.} = 5$ nm, diffracted line from (100) plane, corresponds to *c*-plane oriented columnar grains, can be clearly observed. Therefore, for the media *B*, *c*-plane oriented columnar grains grow from the initial growth stage, which mean $d_{ini.}$ is very thin in the media. In the case of the media *C*, which shows the highest coercivity and squareness compared with the media using other intermediate layer or underlayer, the diffracted lines from (100) plane for both magnetic layer and intermediate layer are overlapped.

Figures 19 show a bright-field image and electron diffraction patterns obtained by cross-sectional TEM for the medium *C* with $Co_{60}Cr_{40}$/C intermediate layer. A high resolution image at the interface between $Co_{67}Cr_{19}Pt_8B_4$ magnetic layer and $Co_{60}Cr_{40}$ layer in the medium *C* is also shown. A spot pattern of electron diffraction images obtained from the columnar structure of b) and c) reveal that preferred orientation of columnar structure is *c*-plane. This is consistent with the in-plane XRD analysis shown in Fig. 18 (*C*). As seen in the high resolution image, layered crystal lattices of *c*-plane continue from the intermediate layer to the magnetic layer, which means the epitaxial-growth of $Co_{67}Cr_{19}Pt_8B_4$ on hcp grains of the $Co_{60}Cr_{40}$ layer. Note that a layer with light gray contrast in the bright field image with the thickness of about 6 nm can be seen in the initial region of the $Co_{60}Cr_{40}$ layer. Judging from the ring pattern of the electron diffraction image of a), this layer consists of nanocrystalline grains whose crystal axes are randomly oriented in three-dimensional space. For the $Co_{67}Cr_{19}Pt_8B_4/Co_{60}Cr_{40}$/C media, it is found that the C seedlayer promotes the formation of Cr-deprived hcp grains with Cr segregation structure in the $Co_{60}Cr_{40}$ intermediate layer, although nanocrystalline layer is formed in the initial growth stage of the $Co_{60}Cr_{40}$ intermediate layer. It is suggested that the Cr-deprived hcp grains in the intermediate layer prevent the formation of initial layer in magnetic layer due to epitaxial growth, which lead to the remarkable improvement of the magnetic properties for the $Co_{67}Cr_{19}Pt_8B_4/Co_{60}Cr_{40}$/C media from the structural point of view [25, 26].

Finally, we pointed out problems left over for CoCr-based perpendicular recording media. Fig. 20 shows the thickness dependence of H_c/H_k^{grain} (lower part) and α (upper part) for $Co_{67}Cr_{19}Pt_8B_4$ media (*A*) without intermediate layer, (*B*) with Ru and (*C*) $Co_{60}Cr_{40}$/C intermediate layer, respectively. The other magnetic properties and microstructure of these media have been shown in Fig. 16-19. As seen, in spite of the elimination of the

initial layer, the maximum value of H_c/H_k^{grain} is no more than 0.31 for the media C with $d_{mag.} = 30$ nm, and this value is lower than that for the medium A (0.32) at $d_{mag.} = 50$ nm. Furthermore, the values of α for the media C are larger than that for the media A, and the values of α for the media C are much larger than 1. These results suggest that the exchange coupling between columnar grains for epitaxial-growth media, which has no initial layer, is stronger compared with that for media having an initial layer. The fact that the exchange coupling increases when the initial layer thickness is decreased, is in agreement with other result which shows that the thinner the initial layer becomes, the stronger exchange coupling tends to be (refer $d_{ini.}$ and α in Figs. 14). Therefore, the key issue of material investigation for CoCr-based perpendicular recording media will be focused on how to fabricate c-plane-oriented columnar grains well-isolated with non-magnetic substance in an epitaxial-growth medium, while maintaining the thermal stability of the medium.

4. Conclusion

We proposed a novel method to evaluate the magnetic properties of the initial layer and the columnar structure separately for CoCr-based perpendicular recording media. We show that the thickness of the initial layer and the intrinsic magnetocrystalline anisotropy of columnar structure can be quantitatively evaluated using the plotted product of perpendicular anisotropy to magnetic film thickness versus magnetic film thickness ($K_{u\perp}^{exp.} \times d_{mag.}$ vs. $d_{mag.}$ plot). Based on the analyses, it is found that: (1) compared with CoCrPtTa media, CoCrPtB media have relatively thin initial layer, and have fine grains with homogeneous columnar structure with c-plane crystallographic orientation; (2) CoCrPtB media can be grown epitaxially on Ru or CoCr/C intermediate layer, and as the result, the magnetic properties of the media within thin thickness region of $d_{mag.} \leq 20$ nm is significantly improved; (3) the key issue of material investigation for CoCr-based perpendicular recording media will be focused on how to fabricate c-plane-oriented columnar grains well isolated with nonmagnetic substance in epitaxial-growth media, while maintaining the thermal stability of the media.

References

[1] e.g. S. Iwasaki and K. Ouchi, IEEE Trans. Magn. **MAG-14**, 849 (1978).
[2] J- G. Zhu and H. N. Bertram, J. Appl. Phys. **66**, 1291 (1989).
[3] A. Takeo, I. Tagawa, and Y. Nakamura, J. Magn. Soc. **19**, 97 (1995).
[4] H. Danan and W. Andra, J. Magn. Magn. Mater. **35**, 299 (1983).
[5] Y. Nakamura and S. Iwasaki, IEEE Trans. Magn. **MAG-23**, 153 (1987).
[6] B. C. Webb, S. Schultz, and S. B. Oseroff, J. Appl. Phys. **63**, 2923 (1988).
[7] A. Lyberatos, R. W. Chantrell, E. R. Sterringa, and J. C. Lodder, J. Appl. Phys. **70**, 4431 (1991).
[8] E. R. Wuory and J. H. Judy, IEEE Trans. Magn. **MAG-20**, 774 (1984).
[9] K. Ouchi and S. Iwasaki, IEEE Trans. Magn. **MAG-23**, 2443 (1987).
[10] M. Takahashi, A. Kikuchi, and S. Kawakita, IEEE Trans. Magn. **33**, 2938 (1997).
[11] K. Omote and S. Matsuno, Advances in X-Ray Chemical Analysis Jpn. **205**, 30 (1999).
[12] A. E. Bell and F. W. Spong, IEEE J. Quantum Electron **14**, 487 (1978).
[13] e.g. Y. Hirayama, M. Futamoto, K. Ito, Y. Honda, and Y. Maruyama, IEEE Trans. Magn. **33**, 996 (1997).
[14] e.g. S. Iwasaki and K. Ouchi, IEEE Trans. Magn. **MAG-14**, 849 (1978).
[15] S. Saito, Y. Hatta, and M. Takahashi, J. Magn. Soc. Jpn. **25**, 587 (2001) (in Japanese).
[16] S. Saito, Y. Hatta, and M. Takahashi, J. Magn. Magn. Mater. **235**, 120 (2001).
[17] D. M. Paige, S. R. Hoon, B. K. Tanner, and K. O'Grady, IEEE Trans. Magn. **MAG-20**, 1852 (1984).
[18] M. Takahashi, T. Shimatsu, M. Suekane, M. Miyamura, K. Yamaguchi, and H. Yamasaki, IEEE Trans. Magn. **28**, 3285 (1992).
[19] S. Saito, Y. Sato, F. Hoshi, and M. Takahashi, J. Magn. Soc. Jpn. **26**, 215 (2002) (in Japanese).
[20] S. Saito, Y. Sato, F. Hoshi, and M. Takahashi, J. Appl. Phys. **91**, 8351 (2002).
[21] S. Saito, D. Hasegawa, D. D. Djayaprawira, and M. Takahashi, J. Magn. Soc. Jpn. **25**, 583 (2001) (in Japanese).
[22] S. Saito, D. Hasegawa, F. Hoshi, D. D. Djayaprawira, and M. Takahashi, Appl. Phys. Lett. **80**, 811 (2001).
[23] S. Saito, F. Hoshi, and M. Takahashi, J. Appl. Phys. **91**, 8028 (2002).
[24] M. Mikami, D. D. Djayaprawira, T. K. Kong, S. Yoshimura, A. Horii, and M. Takahashi, IEEE Trans. Magn. **37**, 1484 (2001).
[25] S. Saito, F. Hoshi, and M. Takahashi, J. Magn. Soc. Jpn. **26**, 210 (2002) (in Japanese).
[26] S. Saito, F. Hoshi, and M. Takahashi, IEEE Trans. Magn. **38**, (2002) (in press).